

On the process-dependence of coherent medium-induced gluon radiation

Stéphane Peigné,^a Rodion Kolevatov^{a,b}

^a*SUBATECH, UMR 6457, Université de Nantes, Ecole des Mines de Nantes, IN2P3/CNRS
4 rue Alfred Kastler, 44307 Nantes cedex 3, France*

^b*Department of High Energy Physics, Saint-Petersburg State University
Ulyanovskaya 1, 198504, Saint-Petersburg, Russia*

E-mail: peigne@subatech.in2p3.fr, kolevato@subatech.in2p3.fr

ABSTRACT: Considering forward dijet production in the $q \rightarrow qg$ partonic process, we derive the spectrum of accompanying soft gluon radiation induced by rescatterings in a nuclear target. The spectrum is obtained to logarithmic accuracy for an arbitrary energy sharing between the final quark and gluon, and for final transverse momenta as well as momentum imbalance being large as compared to transverse momentum nuclear broadening. In the case of equal energy sharing and for approximately back-to-back quark and gluon transverse momenta, we reproduce a previous result of Liou and Mueller. Interpreting our result, we conjecture a simple formula for the medium-induced radiation spectrum associated to hard forward $1 \rightarrow n$ processes, which we explicitly check in the case of the $g \rightarrow gg$ process.

KEYWORDS: parton energy loss; soft gluon radiation; non-universality

Contents

| | | |
|----------|---|----------|
| 1 | Introduction and summary | 1 |
| 2 | Forward single jet production | 2 |
| 2.1 | Review of previous studies | 2 |
| 2.2 | Physical interpretation | 5 |
| 3 | Forward $q \rightarrow qg$ production | 6 |
| 3.1 | Model for $q \rightarrow qg$ hard process | 6 |
| 3.2 | Medium-induced coherent radiation spectrum | 7 |
| 3.3 | Interpretation and conjecture | 9 |

1 Introduction and summary

A few years ago it was emphasized that the medium-induced radiative energy loss ΔE of a high-energy gluon crossing a nuclear medium and being scattered to small angle (in the medium rest frame) is proportional to the gluon energy E [1]. The behavior $\Delta E \propto E$ arises from soft gluon radiation with formation time t_f scaling as E , *i.e.*, being *fully coherent* over the size L of the medium ($t_f \gg L$ at large E). As discussed in Ref. [1], coherent radiative energy loss arises from the interference between emission amplitudes off the incoming and outgoing particles, and is thus expected in all situations where the hard partonic process is effectively equivalent to the forward scattering of an incoming parton to an outgoing compact *colored* system of partons. Coherent energy loss should play an important role in the high-energy *hadro*production of hadrons, but should be absent in (inclusive) Drell-Yan production, as well as in hadron photoproduction. In the case of J/ψ hadroproduction at low $p_\perp \lesssim M_{J/\psi}$, viewed in the target rest frame as the scattering of an incoming gluon to an outgoing *color octet* compact $c\bar{c}$ pair, such a coherent, medium-induced energy loss was shown to provide a successful description of J/ψ nuclear suppression in proton-nucleus (p-A) as compared to proton-proton (p-p) collisions, from fixed-target (SPS, HERA, FNAL) to collider (RHIC, LHC) energies [2–4].

Before studying the possible effect of coherent energy loss on other observables, one should first consider the question of the process dependence of the medium-induced coherent radiation spectrum $\omega dI/d\omega$. Recent studies [5, 6] started to address this question. The radiation spectra associated to $1 \rightarrow 1$ [6] and $1 \rightarrow 2$ [5] forward scattering processes are found to be proportional to the same logarithm of the kinematical parameters, but to possibly differ by an overall factor. For instance, Liou and Mueller showed that the $q \rightarrow qg$ and $g \rightarrow q\bar{q}$ processes, in the kinematics where the outgoing jets have identical longitudinal momenta and nearly back-to-back transverse momenta, lead to the same medium-induced radiation spectrum up to a surprising factor $4/5$ [5].

In the present study, we derive the coherent radiation spectrum associated to the $q \rightarrow qg$ process already studied in [5], but using a different setup. First, we consider the outgoing gluon and quark to carry the fractions x_h and $(1 - x_h)$ of the incoming (light-cone) longitudinal momentum p^+ ($x_h = 1/2$ was chosen in [5]). Second, not only the final gluon and quark transverse momenta $\vec{K}_{1\perp} \equiv \mathbf{K}_1$ and $\vec{K}_{2\perp} \equiv \mathbf{K}_2$, but also their momentum imbalance $\mathbf{K}_1 + \mathbf{K}_2 \equiv \mathbf{q}$, are chosen to be hard compared to the transverse momentum broadening Δq_\perp across the medium, $|\mathbf{K}_1|, |\mathbf{K}_2|, |\mathbf{q}| \gg \Delta q_\perp$. Within this setup, the radiation spectrum associated to $q \rightarrow qg$ is derived in an opacity expansion (as in [6] for $1 \rightarrow 1$ forward processes), and in the large N_c limit (as in [5]). The resulting radiation spectrum is proportional to the same leading logarithm as in Refs. [5, 6], but with a prefactor depending on the hard $q \rightarrow qg$ process through the kinematical variables $x_h, \mathbf{q}, \mathbf{K}_1$. This prefactor is simply interpreted as the probability for the qg pair to be produced in the $\bar{\mathbf{6}} \oplus \mathbf{15}$ subspace of all possible qg color states. For $|\mathbf{q}| \ll |\mathbf{K}_1|$ and $x_h = 1/2$ we recover the factor $4/5$ found in [5]. We conjecture the simple formula (3.22) for the medium-induced radiation spectrum associated to hard forward $1 \rightarrow n$ processes. The conjecture is explicitly verified in the case of the $g \rightarrow gg$ process, where in the particular limit $|\mathbf{q}| \ll |\mathbf{K}_1|$ and $x_h = 1/2$ we find the overall factor $5/3$, instead of $4/5$ for the $q \rightarrow qg$ process.

In section 2 we review the theoretical setup and the results of Refs. [1, 6] for $1 \rightarrow 1$ forward processes, and give a physical interpretation of the main features of the medium-induced coherent radiation spectrum. The setup and calculation are generalized to the hard $q \rightarrow qg$ process in section 3.

2 Forward single jet production

2.1 Review of previous studies

Consider a massless parton of large momentum $p = (p^+, 0, \vec{0}_\perp)$ with $p^+ \equiv 2E$,¹ prepared in the far past and traversing some nuclear medium, see Fig. 1. The final energetic ‘jet’ is ‘tagged’ with a transverse momentum \mathbf{p}' much larger than the nuclear transverse broadening $\ell = \sum \ell_i$ acquired through multiple *soft* scattering. As a consequence \mathbf{p}' must arise dominantly from a *single hard* scattering $\mathbf{q} \simeq \mathbf{p}'$, with $|\mathbf{q}| \gg |\ell|$. We focus on the $p^+ \rightarrow \infty$ limit at fixed transverse momentum (small angle scattering). The fast parton is also assumed to scatter with a negligible longitudinal momentum transfer to the medium, which allows one to neglect the recoil of the target partons. This setup is used in [1, 6] to derive the medium-induced coherent radiation associated to ‘forward single jet’ production (*i.e.*, $1 \rightarrow 1$ forward production), which we briefly review below. In the following, the radiated gluon momentum is denoted by $k = (k^+, \mathbf{k}^2/k^+, \mathbf{k} \equiv \vec{k}_\perp)$, and we focus on soft ($x \equiv k^+/p^+ \ll 1$) and small angle ($|\mathbf{k}| \ll k^+$) radiation (hence $k^+ \equiv \omega + k^z \simeq 2\omega$). As we will see, the main features of coherent radiation induced by $1 \rightarrow 1$ processes also arise for the $1 \rightarrow 2$ process ($q \rightarrow qg$) studied in section 3. This is because coherent radiation, in the limit considered in section 3, effectively sees the ‘dijet’ qg final state as a pointlike object.

¹We use light-cone variables, $p = (p^+, p^-, \mathbf{p})$, with $p^\pm = p^0 \pm p^z$ and $\mathbf{p} \equiv \vec{p}_\perp$.

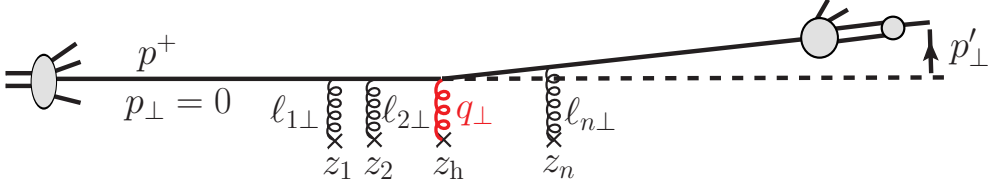


Figure 1. Setup for $1 \rightarrow 1$ forward production used in [1, 6], as viewed in the nuclear target rest frame. The solid line denotes the energetic parton (gluon or quark). The hard process is modeled by a transverse momentum exchange q_\perp (in red) occurring at the longitudinal position z_h , and supplemented by soft rescatterings $\ell_{i\perp} \ll q_\perp$ (with also $\ell_\perp = |\sum \ell_i| \ll q_\perp$) occurring at longitudinal positions z_i .

In Ref. [1] the coherent radiation spectrum dI/dx associated to the $g \rightarrow g$ process (with the final ‘gluon’ being a compact color octet $Q\bar{Q}$ pair of mass M) was derived by modeling the transverse momentum broadening Δq_\perp across the medium by a *single* rescattering ℓ_\perp , and identifying $\ell_\perp^2 = \Delta q_\perp^2(L) = \hat{q}L$, with \hat{q} the transport coefficient. The obtained result,

$$x \frac{dI}{dx} \Big|_{g \rightarrow g} = N_c \frac{\alpha_s}{\pi} \log \left(1 + \frac{\Delta q_\perp^2(L)}{x^2 M_\perp^2} \right), \quad (2.1)$$

where $M_\perp^2 \equiv M^2 + p_\perp'^2 \simeq M^2 + q_\perp^2$, was confirmed in [6] in a theoretical setup using the opacity expansion [7], allowing one to consider an arbitrary number n of soft rescatterings in the medium.

In the present paper we focus on the case of massless particles and, similarly to Ref. [5], on the small- x region where the spectrum is logarithmically enhanced. We thus rewrite (2.1) as

$$x \frac{dI}{dx} \Big|_{g \rightarrow g} = N_c \frac{\alpha_s}{\pi} \left[\log \left(\frac{\Delta q_\perp^2(L)}{x^2 q_\perp^2} \right) + \mathcal{O}(1) \right]. \quad (2.2)$$

We stress that the latter expression holds when not only the argument of the logarithm, but the logarithm itself is much larger than unity, *i.e.*, to *logarithmic accuracy*, which will be implicit throughout our study.

It is useful to recall the basic steps leading to (2.2). It was shown in [6] that the spectrum at order n in the opacity expansion is given by

$$x \frac{dI^{(n)}}{dx} = \frac{\alpha_s}{\pi^2} \int d^2 \mathbf{k} \left[\prod_{i=1}^n \int \frac{dz_i}{C_R \lambda_R} \int d^2 \ell_i V(\ell_i) \right] \frac{\sum \text{[Diagrams]}}{\text{[Diagram]}} \quad (2.3)$$

where the diagrams appearing in the numerator and denominator are evaluated using the pictorial rules defined in Fig. 2. The upper (lower) part of each diagram appearing in the numerator of (2.3) corresponds to a contribution to the emission amplitude (conjugate amplitude) of the soft gluon \mathbf{k} induced by the rescatterings ℓ_i . The diagram in the denominator

(a)

(b)

Figure 2. Pictorial rules for (a) emission vertices and (b) color factors. The energetic parton of color charge C_R is denoted by the solid line ($C_R = C_A = N_c$ for a gluon and $C_R = C_F = (N_c^2 - 1)/(2N_c)$ for a quark). For the pictorial representation of color factors, see for instance Ref. [10].

stands for the hard process ‘cross section’ (which here is a single color factor, other factors cancelling between numerator and denominator). The quantity λ_R is the elastic mean free path of the fast parton of color charge C_R (note that the product $C_R \lambda_R = C_F \lambda_q = N_c \lambda_g$ is independent of the parton type), and an average over soft transfers ℓ_i is performed using the screened Coulomb potential $V(\ell_i) = \mu^2/[\pi(\ell_i^2 + \mu^2)^2]$. The latter provides the typical magnitude of soft transfers, $|\ell_i| \sim \mu \ll |q|$, with μ being the inverse screening length of the medium.

We stress that the evaluation of (2.3) in [6] is done in the *coherent* limit $t_f \gg L$ and assuming $k_\perp \ll q_\perp$, which leads to important simplifications:

- (i) Diagrams where the time t associated to the soft emission vertex is in between two rescatterings, $z_i < t < z_{i+1}$, are negligible.
- (ii) Diagrams where the hard gluon q couples to the soft radiated gluon k are negligible. (The rescattering gluons ℓ_i can couple to both the energetic parton and the soft gluon, including virtual contributions where two gluon lines ℓ_i and $-\ell_i$ are transferred in either the amplitude or conjugate amplitude.)
- (iii) At each order in opacity, the contribution to (2.3) of purely initial state radiation cancels out. (The same holds for purely final state radiation.) Only interference diagrams remain, like the generic diagram drawn in numerator of (2.3).

At first order in opacity we find [6]

$$x \frac{dI^{(1)}}{dx} = (2C_R - N_c) \frac{\alpha_s}{\pi^2} \frac{L}{\lambda_g} \int d^2 \mathbf{k} \int d^2 \ell_1 V(\ell_1) \left[\frac{\mathbf{k} - \ell_1}{(\mathbf{k} - \ell_1)^2} - \frac{\mathbf{k}}{k^2} \right] \cdot \frac{-(\mathbf{k} - x\mathbf{q})}{(\mathbf{k} - x\mathbf{q})^2}, \quad (2.4)$$

which can be interpreted as the interference between the wavefunction of the final parton-gluon fluctuation (the last factor in the integrand of (2.4)), and the incoming ‘medium-induced wavefunction’ (factor in between brackets). For the purpose of the present study, it is sufficient to observe that when $x|q| \ll |\ell_1| \sim \mu$, the spectrum arises from the logarithmic

k_\perp -domain $x|\mathbf{q}| \ll |\mathbf{k}| \ll \mu$, leading to

$$x \frac{dI^{(1)}}{dx} = (2C_R - N_c) \frac{\alpha_s}{\pi} \frac{L}{\lambda_g} \log \left(\frac{\mu^2}{x^2 \mathbf{q}^2} \right). \quad (2.5)$$

The spectrum at all orders in opacity derived in [6] can be formally obtained from (2.5) by shifting the rescattering probability L/λ_g by unity, and the broadening in a *single* scattering μ^2 by the broadening in *multiple* scattering $\Delta q_\perp^2(L) \sim \mu^2 L/\lambda_g \equiv \hat{q}L$. It reads

$$x \frac{dI}{dx} = \sum_{n=1}^{\infty} x \frac{dI^{(n)}}{dx} = (2C_R - N_c) \frac{\alpha_s}{\pi} \log \left(\frac{\Delta q_\perp^2(L)}{x^2 \mathbf{q}^2} \right), \quad (2.6)$$

which in the case of an incoming gluon ($C_R = N_c$) yields the result (2.2).

2.2 Physical interpretation

logarithmic range

At small $x \ll \Delta q_\perp(L)/|\mathbf{q}|$ and to logarithmic accuracy, the spectrum (2.6) arises from the region

$$x|\mathbf{q}| \ll |\mathbf{k}| \ll \Delta q_\perp(L), \quad (2.7)$$

which has a simple physical interpretation.

First, the leftmost inequality is equivalent to saying that at the time $t_f \sim \omega/k_\perp^2$ of its emission, the soft gluon does *not* probe the relative displacement $\Delta \vec{r}$ of the *core* charge compared to the case of unperturbed (vacuum) propagation. Indeed, denoting v_1 (v_2) the velocity of the incoming (outgoing) energetic charge, the latter statement reads [11]

$$1/\omega \gg \Delta r_\parallel = |v_{2\parallel} - v_{1\parallel}| t_f \sim \frac{q_\perp^2}{E^2} \frac{\omega}{k_\perp^2} \quad \text{and} \quad 1/k_\perp \gg \Delta r_\perp = v_{2\perp} t_f \sim \frac{q_\perp}{E} \frac{\omega}{k_\perp^2}, \quad (2.8)$$

which is equivalent to the single condition $xq_\perp \ll k_\perp$. Under such a constraint, no radiation would occur in QED, where only the photon field components which can ‘see’ the deviation of the parent charge can be released as true radiation. In the present QCD situation, the inequality $xq_\perp \ll k_\perp$ thus means that only the purely non-abelian part of radiation contributes to the spectrum. But for this part of radiation to actually contribute to the *medium-induced* spectrum, the soft gluon should probe the transverse displacement Δr_\perp^g of the core charge *proper gluon field* induced by rescatterings. This implies $1/k_\perp \ll \Delta r_\perp^g \sim (\ell_\perp/\omega) t_f$, where ℓ_\perp/ω is the deviation angle of the incoming gluon proper field in the medium. This leads to the second inequality of (2.7). In summary, the range (2.7) can be interpreted as the dominant k_\perp -region for *purely non-abelian, medium-induced* radiation.

color factor

The color factor associated to the coherent radiation spectrum (2.6) can also be simply understood. For a general $1 \rightarrow 1$ process with incoming and outgoing particles in color representations R and R' , respectively, the color factor is $2T_R^a T_{R'}^a$, as can be trivially checked from the structure of the interference terms giving rise to (2.6). Using the identity

$$2T_R^a T_{R'}^a = (T_R^a)^2 + (T_{R'}^a)^2 - (T_R^a - T_{R'}^a)^2 = C_R + C_{R'} - C_t, \quad (2.9)$$

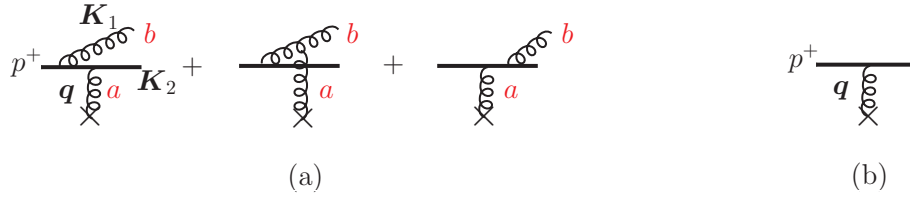


Figure 3. (a) Amplitude for hard $q \rightarrow qq$ production process. (b) Elastic amplitude \mathcal{M}_{el} .

where C_t is the color charge exchanged in the t -channel of the hard process, we recover the factor $2C_R - N_c$ in the case (2.6) of asymptotic parton scattering.² For the processes $q \rightarrow g$ and $g \rightarrow q$ mediated by t -channel color triplet exchange, the color factor reads $C_F + N_c - C_F = N_c$, as found in [6].

3 Forward $q \rightarrow qq$ production

We now consider a simple generalization of section 2, by replacing the $1 \rightarrow 1$ forward hard process by the $q \rightarrow qq$ process, and derive the associated medium-induced soft radiation spectrum.

3.1 Model for $q \rightarrow qq$ hard process

The $q \rightarrow qq$ production amplitude is depicted in Fig. 3a, where the final gluon and quark have transverse momenta $\mathbf{K}_1 \equiv \vec{K}_{1\perp}$ and $\mathbf{K}_2 \equiv \vec{K}_{2\perp}$, and light-cone longitudinal momentum fractions $x_h \equiv K_1^+/p^+$ and $1 - x_h \equiv K_2^+/p^+$, respectively. We consider the $p^+ \rightarrow \infty$ limit at fixed and finite $x_h \sim \mathcal{O}(1)$. The amplitude of Fig. 3a is conveniently derived in a light-cone formalism and in light-cone $A^+ = 0$ gauge.

In scalar QCD, we find

$$\mathcal{M}_{\text{hard}} = \hat{\mathcal{M}}_{el} \cdot 2g(1 - x_h) \cdot \left[T^a T^b \frac{\mathbf{K}_1}{\mathbf{K}_1^2} + [T^b, T^a] \frac{\mathbf{K}_1 - \mathbf{q}}{(\mathbf{K}_1 - \mathbf{q})^2} - T^b T^a \frac{\mathbf{K}_1 - x_h \mathbf{q}}{(\mathbf{K}_1 - x_h \mathbf{q})^2} \right] \cdot \boldsymbol{\varepsilon}_1, \quad (3.1)$$

where $\hat{\mathcal{M}}_{el}$ denotes the Lorentz part (*i.e.*, without color factor) of the elastic amplitude of Fig. 3b, and $\boldsymbol{\varepsilon}_1 \equiv \vec{\varepsilon}_{1\perp}$ the final gluon physical polarization. Since $\boldsymbol{\varepsilon}_1$ formally disappears after squaring the amplitude and summing over the two physical polarization states, it can be dropped in (3.1).

In QCD, the spinor structure makes the amplitude of Fig. 3a slightly more complicated than (3.1).³ However, after squaring, summing over polarization states and over color, the result for $|\mathcal{M}_{\text{hard}}|^2$ in QCD is the same (for a given quark light-cone helicity) as if $\mathcal{M}_{\text{hard}}$ were given by the scalar QCD expression (3.1), up to the replacement of the overall factor

$$1 - x_h \text{ (scalar QCD)} \rightarrow \sqrt{\frac{1 + (1 - x_h)^2}{2}} \text{ (QCD)}. \quad (3.2)$$

²For $q \rightarrow q$ scattering, this factor reads $2C_F - N_c = -1/N_c$, and the medium-induced radiation spectrum associated to $q \rightarrow q$ is thus suppressed in the large N_c limit.

³The QCD calculation can be done using light-cone helicity spinors [8].

Moreover, specific contributions to $|\mathcal{M}_{\text{hard}}|^2$ corresponding to the interference of different graphs of Fig. 3a (including initial and final state radiation) are reproduced one by one with this replacement. We specially emphasize this fact since only part of these contributions enter the calculation of the induced soft radiation spectrum (see section 3.2).

The overall factor is irrelevant for our purpose, since it will cancel between numerator and denominator in the induced soft radiation spectrum (3.6). We can thus use (in either spinor or scalar QCD):

$$\mathcal{M}_{\text{hard}} \propto T^a T^b \frac{\mathbf{K}_1}{\mathbf{K}_1^2} + [T^b, T^a] \frac{\mathbf{K}_1 - \mathbf{q}}{(\mathbf{K}_1 - \mathbf{q})^2} - T^b T^a \frac{\mathbf{K}_1 - x_h \mathbf{q}}{(\mathbf{K}_1 - x_h \mathbf{q})^2}. \quad (3.3)$$

We stress that this expression, derived long ago by Gunion and Bertsch [9],⁴ holds for any *finite* x_h in the $p^+ \rightarrow \infty$ limit.

The amplitude (3.3) will be our model for the hard process. In addition to $x_h \sim \mathcal{O}(1)$, we choose (as in Ref. [5]) \mathbf{K}_1 and \mathbf{K}_2 to be much larger than the nuclear broadening Δq_\perp . However, in view of applying the opacity expansion as in the $1 \rightarrow 1$ case studied in section 2, we also choose the dijet *momentum imbalance* $\mathbf{q} = \mathbf{K}_1 + \mathbf{K}_2$ to satisfy $|\mathbf{q}| \gg \Delta q_\perp$. As a consequence, the dijet imbalance is provided by a single hard exchange \mathbf{q} and negligibly affected by soft rescatterings in the medium. In summary we consider the $q \rightarrow qg$ process in the kinematics

$$x_h \sim \mathcal{O}(1) \quad \text{and} \quad |\mathbf{K}_1|, |\mathbf{K}_2|, |\mathbf{q}| \gg \Delta q_\perp. \quad (3.4)$$

3.2 Medium-induced coherent radiation spectrum

The medium-induced radiation spectrum associated to $q \rightarrow qg$ is derived in the *soft* radiation limit defined by

$$x \equiv \frac{k^+}{p^+} \ll 1 \quad \text{and} \quad k_\perp \ll |\mathbf{K}_1|, |\mathbf{K}_2|, |\mathbf{q}|. \quad (3.5)$$

The calculation is greatly simplified by observing that the hard process structure (3.3) is given by the pictorial rules of Fig. 2. It is then straightforward to show that the radiation spectrum associated to $q \rightarrow qg$ is given, at order n in opacity, by the expression (2.3) with the $1 \rightarrow 1$ replaced by the $q \rightarrow qg$ hard process. For instance, at first order in opacity,

$$x \frac{dI^{(1)}}{dx} \Big|_{q \rightarrow qg} = \frac{\alpha_s}{\pi^2} \int d^2 \mathbf{k} \int \frac{dz_1}{N_c \lambda_g} \int d^2 \boldsymbol{\ell}_1 V(\boldsymbol{\ell}_1) \frac{C}{H}, \quad (3.6)$$

where H and C are given by the diagrams of Figs. 4 and 5, respectively. This calls for several comments:

- (i) As a simplifying assumption, we choose the gluon formation time t_f to be large not only compared to L (as in section 2) but also compared to the hard process production time t_{hard} ,

$$t_f \sim \frac{k^+}{k_\perp^2} \gg t_{\text{hard}} \sim \frac{p^+}{K_{1\perp}^2} \gg L. \quad (3.7)$$

⁴In Ref. [9], the scalar QCD expression (3.1) is given, but used only in the limit $x_h \rightarrow 0$, where the scalar QCD and spinor QCD expressions of $|\mathcal{M}_{\text{hard}}|^2$ coincide (after summing over gluon polarization states).

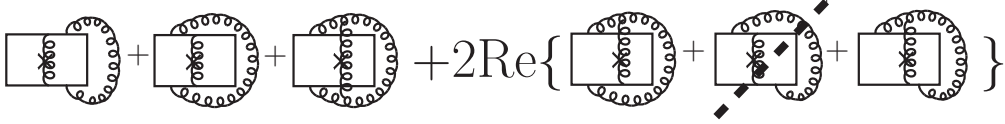


Figure 4. Set H of diagrams corresponding to the $q \rightarrow qq$ hard process, appearing in the denominator of the radiation spectrum (3.6). The barred diagram is suppressed in the large N_c limit.

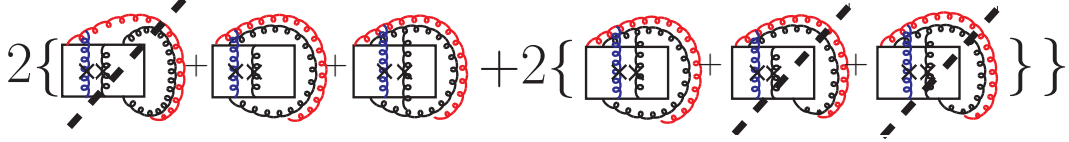


Figure 5. Set C of diagrams (numerator of (3.6)) for soft gluon emission (in red) induced by a single in-medium rescattering (in blue). Among all possible attachments of the rescattering gluon to the hard quark and gluon lines (including virtual contributions where the rescattering gluon couples to two lines in either the amplitude or conjugate amplitude), only one is drawn. Diagrams which are suppressed at large N_c are barred.

In this limit, the dominant diagrams are those (as in the set C of Fig. 5) where the soft gluon emission vertex is either long before or long after the interaction vertices of the hard process shown in Fig. 4. The assumption $t_f \gg t_{\text{hard}}$ constrains the range of validity of our final result (3.11) to the domain (3.14), but still allows for accessing the main features of the induced spectrum.

- (ii) As in the case of $1 \rightarrow 1$ forward processes, diagrams corresponding to purely initial-state or purely final-state radiation cancel out in the medium-induced spectrum. Only interference diagrams remain, where the soft gluon is emitted *before* the hard process in the amplitude, and *after* in the conjugate amplitude (as in Fig. 5).
- (iii) We work in the large N_c limit [12]. In this limit, the interference diagrams where the soft gluon connects to the final quark line are all suppressed, and thus not drawn in Fig. 5. Among the diagrams where the soft gluon connects to the final hard gluon line, those which are suppressed at large N_c are barred in Fig. 5. Note that one diagram contributing to the hard process in Fig. 4 can also be dropped at large N_c .

Applying the pictorial rules of Fig. 2 we find ($\mathbf{K} = \mathbf{K}_1$)

$$H = \frac{N_c^3}{4} \frac{\mathbf{q}^2}{\mathbf{K}^2(\mathbf{K} - \mathbf{q})^2} \left[1 + \frac{(1 - x_h)^2 \mathbf{K}^2}{(\mathbf{K} - x_h \mathbf{q})^2} \right], \quad (3.8)$$

$$C = \frac{N_c^5}{4} \frac{\mathbf{q}^2}{\mathbf{K}^2(\mathbf{K} - \mathbf{q})^2} \left[\frac{\mathbf{k} - \boldsymbol{\ell}}{(\mathbf{k} - \boldsymbol{\ell})^2} - \frac{\mathbf{k}}{\mathbf{k}^2} \right] \cdot \frac{-(\mathbf{k} - \frac{x}{x_h} \mathbf{K})}{(\mathbf{k} - \frac{x}{x_h} \mathbf{K})^2}. \quad (3.9)$$

Inserting the latter expressions in (3.6), we find that to logarithmic accuracy, the spectrum arises from the k_{\perp} -domain $x|\mathbf{K}| \ll |\mathbf{k}| \ll |\boldsymbol{\ell}| \sim \mu$ (recall that $x_h \sim \mathcal{O}(1)$) and reads

$$x \frac{dI^{(1)}}{dx} \Big|_{q \rightarrow qq} = \left[1 + \frac{(1 - x_h)^2 \mathbf{K}^2}{(\mathbf{K} - x_h \mathbf{q})^2} \right]^{-1} \frac{N_c \alpha_s}{\pi} \frac{L}{\lambda_g} \log \left(\frac{\mu^2}{x^2 \mathbf{K}^2} \right). \quad (3.10)$$

The calculation to all orders in opacity can be done as for $1 \rightarrow 1$ processes [6]. Quite intuitively, as was the case for $1 \rightarrow 1$ (see comments after (2.5)), the result is formally obtained by replacing $L/\lambda_g \rightarrow 1$ and $\mu^2 \rightarrow \Delta q_\perp^2(L)$ in the first order result (3.10),

$$x \frac{dI}{dx} \Big|_{q \rightarrow qg} = \sum_{n=1}^{\infty} x \frac{dI^{(n)}}{dx} \Big|_{q \rightarrow qg} = \kappa_{q \rightarrow qg} \frac{N_c \alpha_s}{\pi} \log \left(\frac{\Delta q_\perp^2(L)}{x^2 \mathbf{K}^2} \right), \quad (3.11)$$

$$\kappa_{q \rightarrow qg} \equiv \frac{(\mathbf{K} - x_h \mathbf{q})^2}{(\mathbf{K} - x_h \mathbf{q})^2 + (1 - x_h)^2 \mathbf{K}^2}. \quad (3.12)$$

To logarithmic accuracy, the radiation spectra associated to the $q \rightarrow qg$ and $g \rightarrow g$ hard processes, given in (3.11) and (2.6), are proportional to the same logarithm (up to the renaming of the hard scale $\mathbf{q} \rightarrow \mathbf{K}$ in the logarithm of (2.6)), and otherwise differ by the overall factor $\kappa_{q \rightarrow qg}$ depending on the kinematical variables defining the $q \rightarrow qg$ hard process. In the kinematical situation where $|\mathbf{q}| \ll |\mathbf{K}|$ and $x_h = 1/2$, we recover the factor $\kappa_{q \rightarrow qg} = 4/5$ found in Ref. [5].

Finally, we stress that the result (3.11) arising from the region

$$x K_\perp \ll k_\perp \ll \Delta q_\perp \quad (3.13)$$

was obtained using the assumption (3.7). Our derivation of (3.11) is thus strictly valid provided the condition $t_f \gg t_{\text{hard}}$, or equivalently $x \gg k_\perp^2/K_\perp^2$, holds in the whole domain (3.13). This implies the following validity range of (3.11),

$$\frac{\Delta q_\perp^2}{K_\perp^2} \ll x \ll \frac{\Delta q_\perp}{K_\perp} (\ll 1). \quad (3.14)$$

Let us remark that in Ref. [5] the calculation of the spectrum associated to $q \rightarrow qg$ (done using a different kinematics, namely, small $|\mathbf{q}|$ and $x_h = 1/2$ in our notations) does not assume $t_f \gg t_{\text{hard}}$. Its range of validity is thus broader than the range (3.14) and extends to x -values which are smaller than the lower bound in (3.14). It is likely that the range of validity of the spectrum (3.11) similarly extends beyond (3.14), for any $|\mathbf{q}|$ and x_h . However keeping track of contributions with $t_f \lesssim t_{\text{hard}}$ would greatly complicate our calculation.

3.3 Interpretation and conjecture

Here we give a simple interpretation of the factor $\kappa_{q \rightarrow qg}$ (given in (3.12)), as well as of the color factor N_c appearing in front of the logarithm in (3.11).

For $N_c \geq 3$, the final quark-gluon pair produced in the hard $q \rightarrow qg$ process can be in three different irreducible color representations,

$$\mathbf{3} \otimes \mathbf{8} = \mathbf{3} \oplus \bar{\mathbf{6}} \oplus \mathbf{15}, \quad (3.15)$$

where the names of the representations indicate their dimensions in the particular case $N_c = 3$. For general N_c the three representations have dimensions

$$K_3 = N_c, \quad K_6 = \frac{N_c(N_c - 2)(N_c + 1)}{2}, \quad K_{15} = \frac{N_c(N_c + 2)(N_c - 1)}{2}, \quad (3.16)$$

and Casimir operators

$$C_3 = \frac{N_c^2 - 1}{2N_c}, \quad C_6 = \frac{(N_c - 1)(3N_c + 1)}{2N_c}, \quad C_{15} = \frac{(N_c + 1)(3N_c - 1)}{2N_c}. \quad (3.17)$$

We observe that the diagrams of Fig. 5 which are suppressed in the large N_c limit are those where the final qg pair is produced in the fundamental representation $\mathbf{3}$. This is not surprising, since we have seen in section 2 that the coherent radiation associated to the $q \rightarrow q$ process is suppressed at large N_c (see footnote 2). Thus, in Fig. 5 (and in Fig. 5 only, see the comments below) we may remove from the beginning the ‘triplet’ component of the final qg pair (or equivalently, project the latter on the $\bar{\mathbf{6}} \oplus \mathbf{15}$ subspace). At large N_c , this is simply achieved by replacing $T^b T^a \rightarrow 0$ in (3.3), leaving $T^a T^b$ unchanged. The hard production amplitude with the final quark-gluon triplet component *removed* thus reads

$$\mathcal{M}_{\text{hard}}^{\bar{\mathbf{6}} \oplus \mathbf{15}} \propto T^a T^b \left(\frac{\mathbf{K}}{K^2} - \frac{\mathbf{K} - \mathbf{q}}{(\mathbf{K} - \mathbf{q})^2} \right). \quad (3.18)$$

Squaring this we find

$$|\mathcal{M}_{\text{hard}}^{\bar{\mathbf{6}} \oplus \mathbf{15}}|^2 = \frac{N_c^3}{4} \frac{q^2}{K^2 (\mathbf{K} - \mathbf{q})^2}, \quad (3.19)$$

and dividing by the expression (3.8) we get

$$\frac{|\mathcal{M}_{\text{hard}}^{\bar{\mathbf{6}} \oplus \mathbf{15}}|^2}{|\mathcal{M}_{\text{hard}}|^2} = \frac{(\mathbf{K} - x_h \mathbf{q})^2}{(\mathbf{K} - x_h \mathbf{q})^2 + (1 - x_h)^2 K^2} = \kappa_{q \rightarrow qg}. \quad (3.20)$$

Thus, the factor $\kappa_{q \rightarrow qg}$ is interpreted as the probability that the quark-gluon pair produced in $q \rightarrow qg$ is *not* in the ‘triplet’ color representation.

Thus, the dependence of the spectrum (3.11) on the hard process kinematical variables \mathbf{q} , \mathbf{K} , x_h , arises from the constraint that at large N_c , only non-triplet qg pairs can contribute to the set C of diagrams (Fig. 5). This ‘selection’ of the $\bar{\mathbf{6}} \oplus \mathbf{15}$ subspace is due to the specific connection of the soft radiated gluon between initial and final state in Fig. 5. In particular, it would be incorrect to attribute this effect to the smaller dimension $K_3 = N_c$ of the triplet representation as compared to the dimension of the $\bar{\mathbf{6}} \oplus \mathbf{15}$ subspace ($K_6 + K_{15} = N_c^3$ at large N_c). For instance, the lower dimension of $\mathbf{3}$ does not prevent the qg pair to be produced as a triplet in the hard $q \rightarrow qg$ process (see set H of diagrams, Fig. 4), even at large N_c .

The logarithmic range (3.13) can be interpreted in a similar way as the range (2.7) for $1 \rightarrow 1$ processes (see section 2.2). Moreover, in the present $q \rightarrow qg$ case, the condition $xK_\perp \ll k_\perp$ written as $1/k_\perp \gg \Delta r_\perp \sim v_\perp t_f \sim (K_\perp/E) \cdot (\omega/k_\perp^2)$ (similarly to (2.8)) means that at the time of its emission, the radiated gluon does not probe the transverse size Δr_\perp of the qg pair. From the point of view of soft radiation, the qg pair thus behaves as an effectively pointlike system.

Finally, the color factor N_c in (3.11) can be simply understood from the rule (2.9). Indeed, since coherent radiation arises from a kinematical domain where the qg pair is effectively pointlike, the result should depend on its *total* color charge, not on the color of its separate constituents. Since the color state of the final qg pair in Fig. 5 is either $\bar{\mathbf{6}}$

or **15**, and these two representations have the same Casimir operator at large N_c , namely $3N_c/2$, the rule (2.9) gives ($R' = \bar{\mathbf{6}}$ or **15**)

$$2T_{\mathbf{3}}^a T_{R'}^a = C_{\mathbf{3}} + C_{R'} - C_{\mathbf{8}} = \frac{N_c}{2} + \frac{3N_c}{2} - N_c = N_c. \quad (3.21)$$

A conjecture

Guided by the above interpretation of our result, we conjecture the following simple formula for the medium-induced radiation spectrum associated to hard forward $1 \rightarrow n$ processes (where the n final-state partons have finite longitudinal momentum fractions $x_i = K_i^+/p^+ \sim \mathcal{O}(1)$ and transverse momenta \mathbf{K}_i of similar magnitude $\sim |\mathbf{K}|$),

$$x \frac{dI}{dx} \Big|_{1 \rightarrow n} = \left[\sum_{R'} P_{R'} (C_R + C_{R'} - C_t) \right] \frac{\alpha_s}{\pi} \log \left(\frac{\Delta q_{\perp}^2(L)}{x^2 \mathbf{K}^2} \right), \quad (3.22)$$

with C_R and C_t the color charges of the incoming parton and of the t -channel exchange, and $P_{R'}$ the probability for the (effectively pointlike) n -parton state to be produced in the color representation R' in the hard process. ($P_{R'}$ may depend on the kinematical variables x_i, \mathbf{K}_i defining the hard $1 \rightarrow n$ process, as in the $q \rightarrow qg$ case.)

As a first illustration, the spectrum associated to $g \rightarrow q\bar{q}$ derived in Ref. [5] can be obtained from (3.22) by setting $P_{R'} = P_{\mathbf{8}} = 1$ (at large N_c the final $q\bar{q}$ is color octet with unit probability) and $C_R = C_{R'} = C_t = N_c$. Not surprisingly, since the final $q\bar{q}$ is effectively pointlike, the result is the same as for the $g \rightarrow g$ process considered in Refs. [1, 6].

As a second example, let us mention that we explicitly verified (3.22) in the case of the $g \rightarrow gg$ process. Using the same theoretical setup (including the large N_c limit) and following the same procedure as for the $q \rightarrow qg$ process, we find an expression for the radiation spectrum similar to (3.11), but with a different overall factor κ ,

$$x \frac{dI}{dx} \Big|_{g \rightarrow gg} = \kappa_{g \rightarrow gg} \frac{N_c \alpha_s}{\pi} \log \left(\frac{\Delta q_{\perp}^2(L)}{x^2 \mathbf{K}^2} \right), \quad (3.23)$$

$$\kappa_{g \rightarrow gg} \equiv 1 + \frac{(\mathbf{K} - x_h \mathbf{q})^2}{(\mathbf{K} - x_h \mathbf{q})^2 + x_h^2 (\mathbf{K} - \mathbf{q})^2 + (1 - x_h)^2 \mathbf{K}^2}. \quad (3.24)$$

(Note that $\kappa_{g \rightarrow gg} = 5/3$ when $|\mathbf{q}| \ll |\mathbf{K}|$ and $x_h = 1/2$.) To check whether (3.23), (3.24) coincide with (3.22), we must sum in (3.22) over the different representations R' of the final gg pair. At large N_c , a two-gluon system can be in six color representations [13],

$$\mathbf{8} \otimes \mathbf{8} = \mathbf{8}_a \oplus \mathbf{10} \oplus \mathbf{1} \oplus \mathbf{8}_s \oplus \mathbf{27} \oplus \mathbf{0}, \quad (3.25)$$

where as in (3.15) the representations are labelled according to their dimensions in the case $N_c = 3$. In particular $\mathbf{0}$ is a symmetric representation which is absent when $N_c = 3$. For $N_c > 3$ the representations appearing in the r.h.s. of (3.25) have the Casimir operators $N_c, 2N_c, 0, N_c, 2(N_c + 1)$ and $2(N_c - 1)$, respectively [13]. Thus, at large N_c the bracket in (3.22) reads

$$\sum_{R'} P_{R'} (C_R + C_{R'} - C_t) = \sum_{R'} P_{R'} C_{R'} = (2 - P_{\mathbf{8}_a} - P_{\mathbf{8}_s}) N_c, \quad (3.26)$$

where we used $C_R = C_t = N_c$, probability conservation $\sum_{R'} P_{R'} = 1$, and the fact that the probability P_1 for the final gg pair to be color singlet is suppressed at large N_c . The probability $P_8 \equiv P_{8_a} + P_{8_s}$ to produce a *color octet* gg pair can be simply evaluated using pictorial rules for the projection operators on specific color representations [13]. Analogously to what was done in (3.20) the calculation gives

$$P_8 = \frac{|\mathcal{M}_{g \rightarrow gg}^{8_a}|^2 + |\mathcal{M}_{g \rightarrow gg}^{8_s}|^2}{|\mathcal{M}_{g \rightarrow gg}|^2} = \frac{x_h^2(\mathbf{K} - \mathbf{q})^2 + (1 - x_h)^2 \mathbf{K}^2}{(\mathbf{K} - x_h \mathbf{q})^2 + x_h^2(\mathbf{K} - \mathbf{q})^2 + (1 - x_h)^2 \mathbf{K}^2}. \quad (3.27)$$

Plugging (3.27) in (3.26), we see that the expression (3.22) reproduces Eqs. (3.23), (3.24). This completes the check of the conjectured expression (3.22) in the case of the $g \rightarrow gg$ process.

Acknowledgments

S.P. would like to thank Tseh Liou and Al Mueller for a rich and instructive correspondence, which motivated the present study. We also thank François Arleo for useful discussions and comments on the manuscript. Feynman diagrams have been drawn with the JaxoDraw software [14]. This work is funded by “Agence Nationale de la Recherche” under grant ANR-PARTONPROP.

References

- [1] F. Arleo, S. Peigné, and T. Sami, *Revisiting scaling properties of medium-induced gluon radiation*, *Phys. Rev.* **D83** (2011) 114036, [[arXiv:1006.0818](#)].
- [2] F. Arleo and S. Peigné, *J/ψ suppression in p -A collisions from parton energy loss in cold QCD matter*, *Phys. Rev. Lett.* **109** (2012) 122301, [[arXiv:1204.4609](#)].
- [3] F. Arleo and S. Peigné, *Heavy-quarkonium suppression in p -A collisions from parton energy loss in cold QCD matter*, *JHEP* **03** (2013) 122, [[arXiv:1212.0434](#)].
- [4] F. Arleo, R. Kolevatov, S. Peigné, and M. Rustamova, *Centrality and p_\perp dependence of J/ψ suppression in proton-nucleus collisions from parton energy loss*, *JHEP* **1305** (2013) 155, [[arXiv:1304.0901](#)].
- [5] T. Liou and A. H. Mueller, *Parton energy loss in high energy hard forward processes in proton-nucleus collisions*, [arXiv:1402.1647](#) [hep-ph].
- [6] S. Peigné, F. Arleo and R. Kolevatov, *Medium-induced gluon radiation: an update*, [arXiv:1402.1671](#) [hep-ph].
- [7] M. Gyulassy, P. Lévai, and I. Vitev, *Reaction operator approach to non-abelian energy loss*, *Nucl. Phys.* **B594** (2001) 371–419, [[nucl-th/0006010](#)].
- [8] G. P. Lepage and S. J. Brodsky, *Exclusive Processes in Perturbative Quantum Chromodynamics*, *Phys.Rev.* **D22** (1980) 2157.
- [9] J. F. Gunion and G. Bertsch, *Hadronization by color bremsstrahlung*, *Phys. Rev.* **D25** (1982) 746.
- [10] Y. L. Dokshitzer, *Perturbative QCD (and beyond)*. In *Lenz, F. (ed.) et al.: Lectures on QCD* 87-135.

- [11] Y. L. Dokshitzer, *Perturbative QCD for beginners*. In *Dubna 1995, High energy physics* 59-120.
- [12] G. 't Hooft, *A Planar Diagram Theory for Strong Interactions*, *Nucl.Phys.* **B72** (1974) 461.
- [13] Y. .L. Dokshitzer and G. Marchesini, *Hadron collisions and the fifth form-factor*, *Phys. Lett. B* **631** (2005) 118 [[hep-ph/0508130](#)].
- [14] D. Binosi, J. Collins, C. Kaufhold, and L. Theussl, *JaxoDraw: A Graphical user interface for drawing Feynman diagrams. Version 2.0 release notes*, *Comput.Phys.Commun.* **180** (2009) 1709–1715, [[arXiv:0811.4113](#)].